ISSN 1726-5749

SENSORS & TRANSDUCERS

vol. 90 Special 4/08

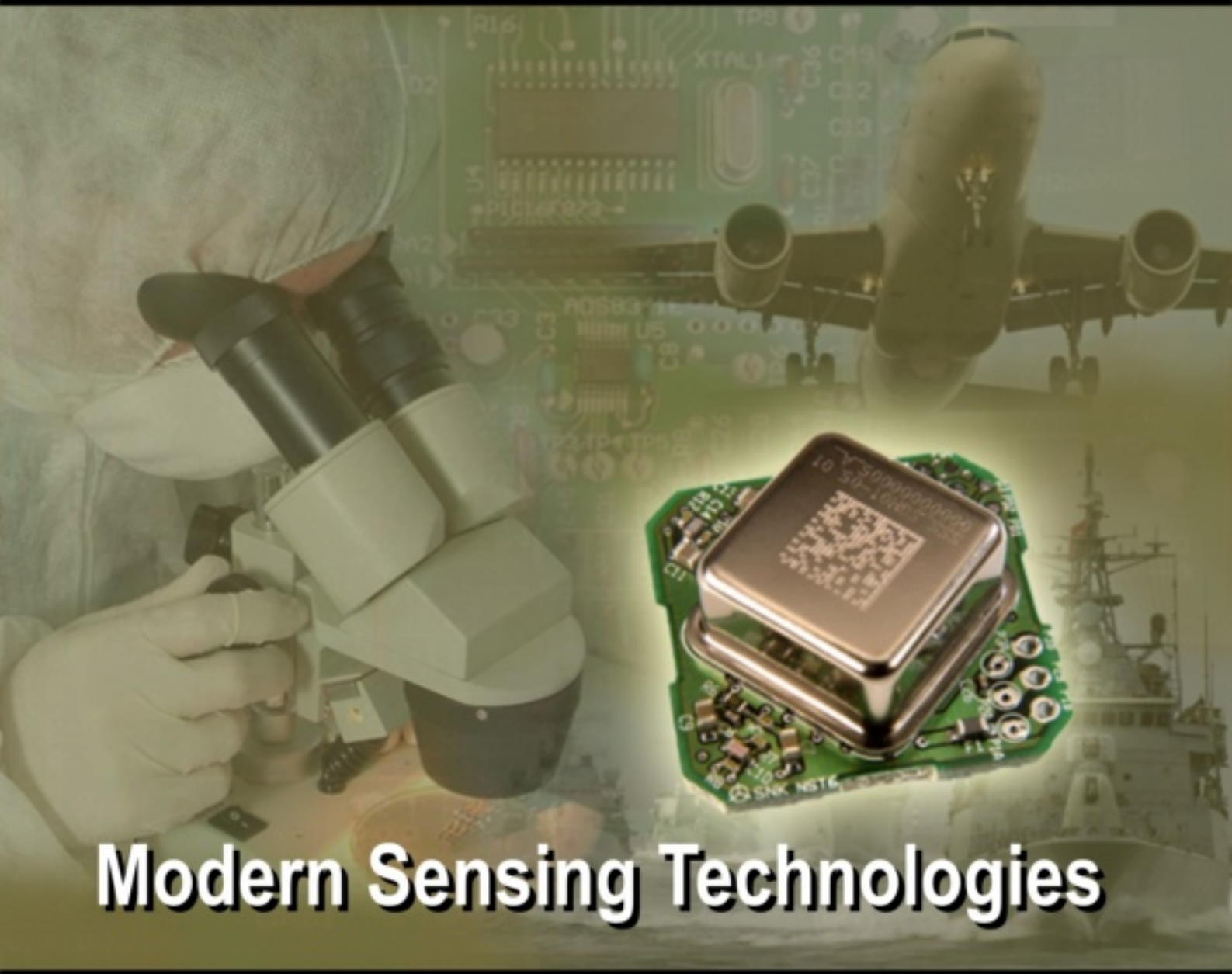

Modern Sensing Technologies

International Frequency Sensor Association Publishing

IFSA

Sensors & Transducers

Special Issue
April 2008

www.sensorsportal.com

ISSN 1726-5479

Sensors & Transducers Journal (ISSN 1726-5479) is a peer review international journal published monthly online by International Frequency Sensor Association (IFSA). Available in electronic and CD-ROM.

Sensors & Transducers Journal

Contents

Volume 90
Special Issue
April 2008

www.sensorsportal.com

ISSN 1726-5479

Special Issue on Modern Sensing Technologies

Sensors Signal Processing

Gas Sensors

Image Sensors

Miscellaneous

Authors are encouraged to submit article in MS Word (doc) and Acrobat (pdf) formats by e-mail: editor@sensorsportal.com
Please visit journal's webpage with preparation instructions: http://www.sensorsportal.com/HTML/DIGEST/Submition.htm

Sensors & Transducers Journal, Vol. 90, Special Issue, April 2008, pp. 310-324

www.sensorsportal.com

Sensors & Transducers

ISSN 1726-5479

http://www.sensorsportal.com

Slip Prediction through Tactile Sensing

[1]Somrak PETCHARTEE and [2]Gareth MONKMAN

[1]Technik Autonomer System, Universität der Bundeswehr, Germany

[2]Mechatronics Research Unit, Fachhochschule Regensburg, Germany

E-mail: somrak.petchartee@gmail.com

Received: 15 October 2007 /Accepted: 20 February 2008 /Published: 15 April 2008

Abstract: This paper introduces a new way to predict contact slip using a resistive tactile sensor. The prototype sensor can be used to provide intrinsic information relating to geometrical features situated on the surface of grasped objects. Information along the gripper finger surface is obtained with a measurement resolution dependant on the number of discrete tactile elements. The tactile sensor predicts the partial slip of a tactile surface by sensing micro vibrations in tangential forces which are caused by an expansion of the slip regions within the contact area. The location of the local slip is not specified but its occurrence can be predicted immediately following micro vibration detection. Predictive models have been used to develop a set of rules which predict the slip based on fluctuations in tactile signal data. *Copyright © 2008 IFSA.*

Keywords: Slip prediction, Pre-slip sensing, Tactile sensor, Minimum grasping force

1. Introduction

Many different slip sensor solutions have been investigated by a number of researchers with limited success. Although today there are still no real slip sensors included in any commercially available hand [1], the idea of including them into a design can be traced back to 1960s [2]. During the design of artificial skins, some researchers have analyzed the mechanical behaviour of human finger skin with ridged surfaces [3]. Yamada et al. used a tactile sensor with surface ridges to measure slip vibrations. He showed a slip sensor that has elastic ridges on the surface and is capable of isolating a stick-slip vibration due to a total slip between sensor and grasped object. The sensor can detect the total slip and control the grasping force quickly and correctly to avoid premature release of an object. However, the method is not adequate because the position of the object will slightly change due to the occurrence of total slip. Measuring normal and tangential forces has also been used to detect slip [4]. Melchiorri's

sensor comprises an integrated sensor consisting of a strain gauge force/torque sensor and a matrix tactile sensor.

Tactile data contains information about magnitudes, distributions and locations of forces. It also provides information about the contact area and the pressure distribution over it. With resistive tactile sensors, changes in electrical resistance can be detected which result from mechanical strains in electrically conductive foam. The soft, deformable surface detects continuous pressure with excellent sensitivity and resolution. The electrical conductivity measured between two electrodes on the same side of the conductive foam (one tactile element) is derived from a number of simultaneously conducting paths. Within this research tactile sensors have been developed with the following specifications: One finger consists of two 16x4 cells, two 16x2 cells, and one 6x2 cells, making up the total 408 cells for the two fingers. The width of the fingers is 20 mm, their length is 55 mm excluding an aluminum core and they have a thickness of 12 mm.

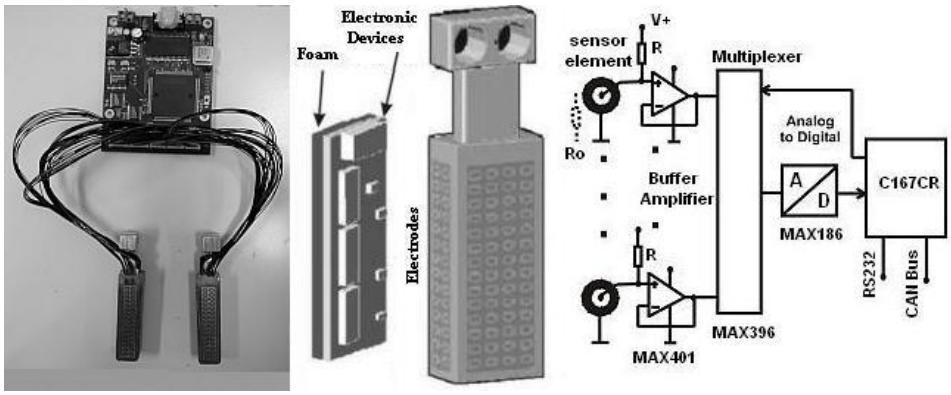

Fig. 1. Electronic assembly.

A tactile element or "taxel", necessary to measure the (local) electrical resistance of the conductive foam, consists of one electrode and a common ground. A constant voltage is applied to a voltage divider circuit between fixed value resistors and the foam at one electrode. By measuring the voltage across the electrodes it is possible to compute the resistance, and consequently the force locally applied to the foam. A 32-bit microcontroller, sampling circuits and memory are installed in the control unit. The micro-controller also has an analogue-multiplexer for accessing all 408 tactile elements. Stack memory is implemented inside the micro-controller by software for data manipulation. Initially, the micro-controller briefly obtains data from the tactile elements independently. Secondly, the tactile data are collected by the stack memory and the micro-controller accesses the remaining tactile elements again by controlling the multiplexer chip. When all tactile elements have been read by the micro-controller, then the micro-controller calculates several parameters which describe the features of the contact points. “Higher-order processing” is implemented on an external computer. This prototype sensor can be used to provide intrinsic information of interest relating to grasped objects, such as geometrical features situated on the object surface. Information along the sensor surface can be obtained by a discrete number of tactile elements to enhance the measurement resolution. Feature heights are detectable down to 3 mm. Each tactile element can be calibrated to act as a force sensing element. The effective pressure detection threshold of a tactile finger is about 50 g/mm^2, giving a normal indentation of skin surface of 0.1 mm (about 3.3 % strain).

Hysteresis is calculated from a stress-strain curve. Hysteresis is the difference between the loading energy and the unloading energy, whereby energy values are determined by calculating the area under the test curve. In the experiment, the sensor was loaded incrementally from 0 to 3 Newtons and then back down to the no load condition to determine the extent of the hysteresis. Fig. 2 shows the resulting

data. The lower curve represents the sensor output for an applied force increased over a period of 1 minute. The upper curve represents a decreasing force over the same time period. The difference between the two curves is the hysteresis, which can be seen to have a maximum of 8.2 % of the total response. This difference lies within the noise range of the system. Consequently, it should be possible to reduce the effect of hysteresis down to an acceptable level by compensation in software.

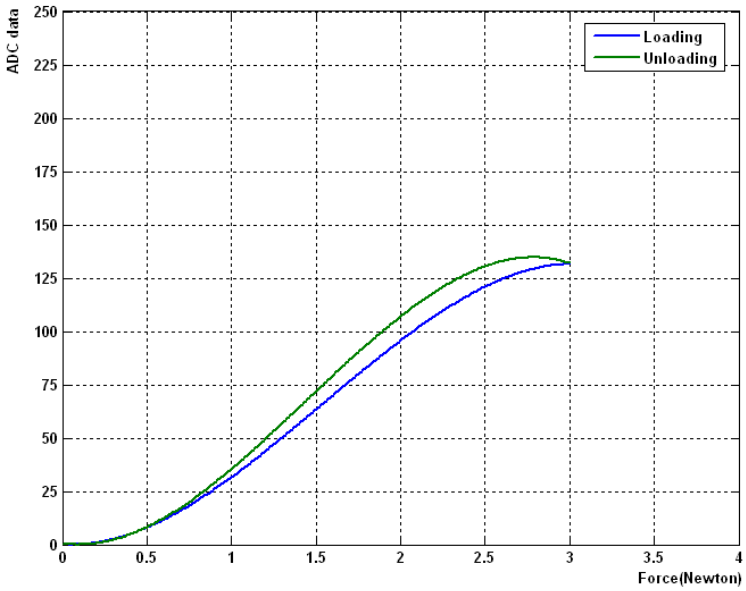

Fig. 2. Hysteresis curve.

The spatial resolution of the sensor is limited by the space between the tactile element centers and the elastomeric properties of the protective material covering the fingerplate. For a sensor which records only the surface normal force, a point source should be detected by only one or more cells directly in contact with the stimuli. In addition, spreading to and blurring from adjacent cells should be minimal because a sharp sensor response provides more detail of the tactile force outlines of an object. Fig. 3 shows the response of a single tactile element when the indentor was used to scan a straight line across the surface. By pressing the indentor to a depth of 1 mm on the tactile surface, data were measured and collected from the eighth taxel located in the middle of the fingerplate. The tactile response changed with the indentors position due to underlying continuum mechanics of the foam media. It showed the peak forming of signals around the area of contact. This was because the distance between tactile elements was held constant at 2 mm. From this, the indentation depth could be determined to be about 1 mm. The number of contacts included 16-grid points with their centroid at the eighth point measured from a coordinate located at the middle of the fingerplate. It can be seen from Fig. 3 that the tactile sensor could discriminate between simultaneous contact points whose distance apart was at least 2 mm. This means if there are any contact points whose distances are less than 2 mm, the tactile sensor will sense them as one contact point. Tactile data not only contain information about magnitudes, directions and locations of forces but also provide information about the contact area and the pressure distribution over it.

Fig. 4 shows variations in the contact resistance when forces are applied to the tactile sensor surface. In the experiment, a 3-mm x 20-mm x 55-mm piece of foam was placed on a flat surface. The indentor was then used to depress the foam. Forces of 2, 4, 6 and 8 Newton applied to the foam surface yielded resistances of 650KΩ, 250KΩ, 100KΩ and 50KΩ respectively, as shown graphically in the force-resistance relationship of Fig. 4. The response was monotonic, although not perfectly linear, for small forces of between 0 and 4 Newtons. The measured values showed that this tactile sensor had a high sensitivity within this range and a lower sensitivity to increasing forces outside of this range.

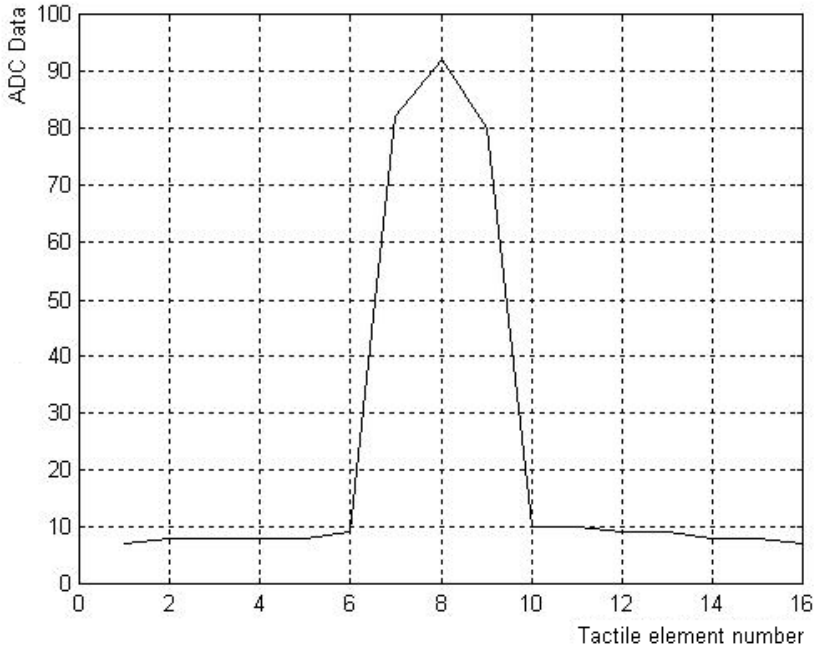

Fig. 3. Single tactile response to lateral scans.

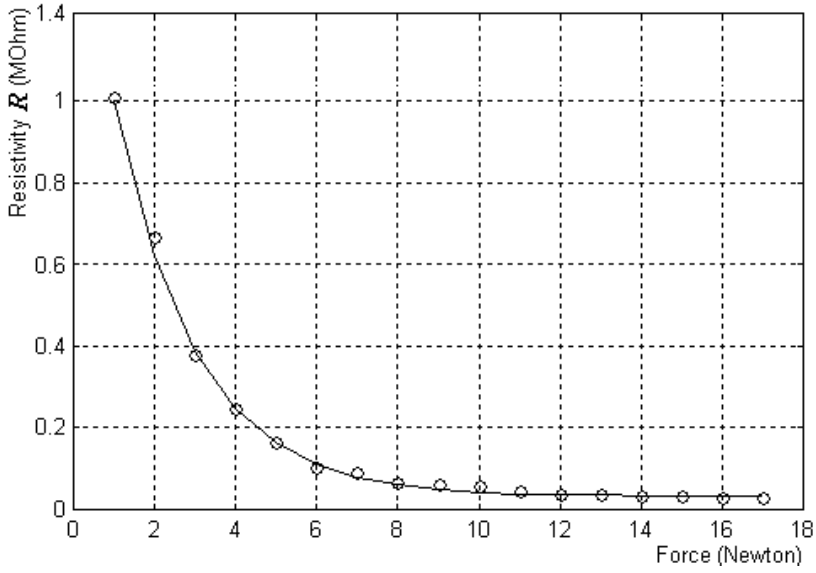

Fig. 4. The relationship between force and electrical resistance.

2. Tactile Sensor for Robot Manipulation

Various factors, including environmental influences, must be considered in order to manipulate an object and prevent it from slipping when external loads exceed the frictional prehension forces. When an object is retained in the human hand, gripping forces are adjusted according to the object's weight and surface friction [6]-[8].

To determine whether similar mechanisms would be of help in the control of robot manipulation tasks, Howe [9], [10] applied hypotheses from human studies to robotic systems. The robotic Grasp-Lift-Replace task involves five phases: approach, loading, manipulation, unloading, and release, linked

together by four contact events. A change in the contact events marks the transition from one phase to another. Robotic tactile sensors described in [9] and [11] detect the contact events and trigger the transitions through the phases of the Grasp-Lift-Replace task. The specialized sensors detect slip during finger to object contact. In addition, information concerning vibration, helpful to contact event identification, is also obtained.

Specifically, the proposed tactile sensor is applied in grasp experimentation by identifying the least force required for prehension. Two experiments are conducted (Fig.5). In the first experiments, the object is retained between the robot fingers above the surface. Prehension forces are then reduced until the first occurrence of pre-slip is detected and the applied force noted as the minimum retention force. In the second experiments, an object, placed on a surface is prehended by a robot and the minimum retention force determined by active force variation. This experiment is divided into phases. In each phase, the signals sensed by the tactile sensors and the techniques used in controlling it are presented.

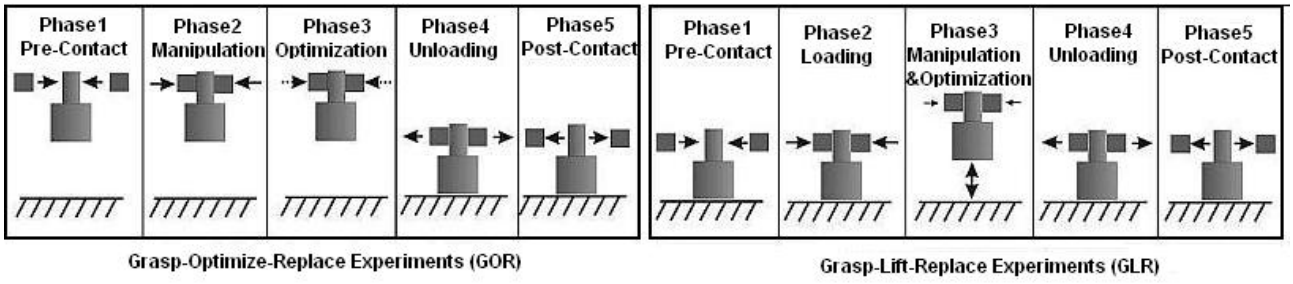

Fig. 5. Grasp-Optimize-Replace Experiments (GOR) and Grasp-Lift-Replace Experiments (GLR).

If tactile sensing is to be the sole source of feedback in controlling a contact task, it must be possible to characterize the task in terms of variables that can be observed using tactile sensing. Furthermore, it must be possible to regulate these variables through the actions of the robot manipulator. The tactile interaction has been implemented on a real system consisting of a manipulator arm having 6 DOFs as shown in Fig. 6. The tactile sensor arrays are mounted on the gripper fingers. The prehended object is a solid cylinder having a mass of 420 grams.

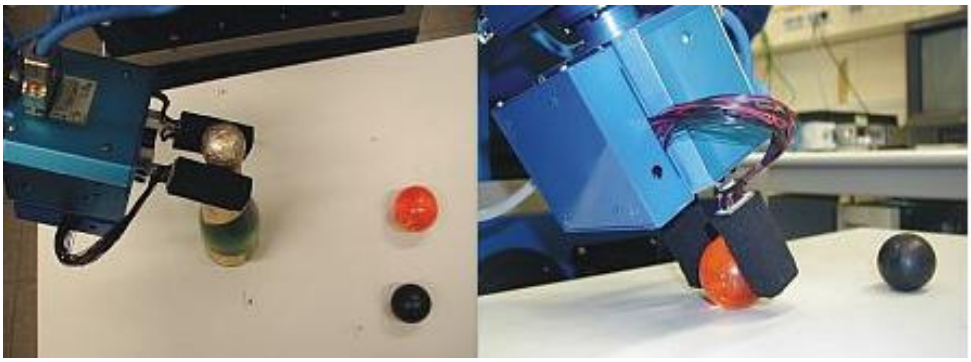

Fig. 6. Robotic Manipulator.

3. The Contact Model and Application

Fluctuations in tactile data are observed within a time interval during which a sequence of stresses is cyclically applied to the specimen at the contact point. The stress waves are generally triangular, square, or sinusoidal, and the typical cycles of stress are reverse stresses, fluctuating stresses, and irregular or random stresses [12].

An understanding of the nature of physical contacts will aid in analyzing robotic prehension. When two objects come into contact, they will exert forces at the contact point. The z-axis is the axis parallel to the normal contact point n and normal forces are represented by F_n. Contact friction forces perpendicular to the normal force are represented by F_t. Contact friction forces on the x and y axes are represented by F_x and F_y, respectively. The relationship between contact friction forces and the normal force on the contact plane are represented in (1) below.

$$F_x^2 + F_y^2 \le \mu^2(x, y) F_n^2, \tag{1}$$

However, in this study the coefficient of friction $\mu(x, y)$ is a function of the coordinate system, which is different from Amantons' friction law [13]. The surface contact between two objects results in a temporary elastic deformation, whose magnitude depends on the size of the applied force. Permanent, plastic deformations do not normally occur during robotic manipulation and will not be considered in this model. When the contact area is small, frictional forces on the surface are high, expanding the contact area due to its deformability. If the local direct stress σ_v is set as a constant, the area receiving the pressure N_i will be equal to $A_i = N_i / \sigma_v$. Thus, the total area under stress will be:

$$A_T = A_1 + A_2 + ... + A_i = \frac{N_1}{\sigma_v} + \frac{N_2}{\sigma_v} ... + \frac{N_i}{\sigma_v} = \frac{N}{\sigma}, \tag{2}$$

where N represents the vector sum of all the normal forces. For hard objects, the actual contact area will be proportional to the magnitude of the force. However, the situation becomes more complicated with less rigid, compliant viscoelastic surfaces such as the polymer foams used in simple tactile sensors. However, in many cases the frictional forces involved in the viscoelastic deformation of polymeric materials have non-linear components which cannot be calculated using the above equations. In addition, the deformation does not only depend on the size of the normal force N but also on its direction and length, which in turn depends on the shape of the object in contact. If the deformation and the degree of force are held constant, then the contact area can be represented by the formula N^{β}. As an illustration, for an elastic rubber-like solid $\beta = 2/3$ [14], this is a general characteristic of most polymers. Howell's equation [15] for frictional force can be reorganized as $F = (KN^{\beta-1})N$, where $(KN^{\beta-1})$ is assumed to be equal to the coefficient of friction μ_0. This equation shows the complexity of the relationship between the normal force and the coefficient of friction μ_0, which consists of two variables. The effective coefficient of friction will reduce as the size of the exerted force increases. In other words, the compressive area has a lower coefficient of friction than the tensile area.

The generation of roughness induced dynamic grasping at a deformable contact may be viewed most simply in the context of the model shown in Fig. 7. Qualitative models to describe the behaviour of a typical polymer will now be introduced. The Kelvin-Voigt model gives retarded elastic behaviour which represents a crosslinked polymer. The Maxwell model gives steady state creep typical of an uncured polymer. With the composition model as shown, it can describe both types of behaviour. The

models are simple and suitable for experimental representation of almost any polymer foam over an extended period of time.

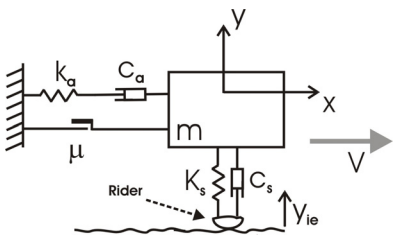

Fig. 7. Dynamic model [16].

The smooth rider in Fig. 7 sits in contact with a rough surface moving at a constant velocity V. The rider is connected to a frame through a suspension characterized by a spring stiffness k_a, a damping constant c_a and a degree of static friction μ. The normal contact stiffness k_s and any associated damping c_s are lumped between the mass and the moving surface. The normal stiffness, linearized about the mean rider position, can be computed from traditional Hertzian theory. With regard to constant friction, the argument is that in order for friction to change, the real contact area, and thus the mean normal separation, of the surface must change [16]. Efforts to verify this were made by Godfrey [18] who demonstrated a reduction in friction due to normal vibration. With the measured frictional shear force being a function of real contact area, an apparent reduction in friction in the presence of normal vibrations can be expected. The idea was that normal vibrations could influence the mean surface separation and hence the real area of contact.

The two models in Fig. 7 can be applied to explain the operation of robot gripper fingers covered by such tactile sensor arrays, as shown in Fig. 8 where (a) side views of the prehension operation can be seen. Fig. 8 (b) shows the maximum deformation of the tactile sensor surface when the object is normal to the motion of the gripper jaws.

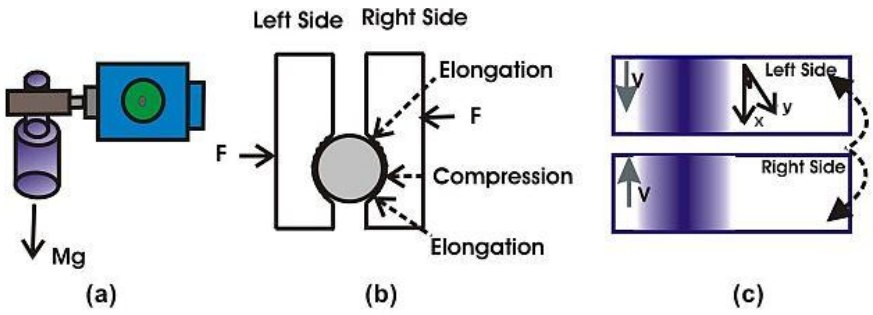

Fig. 8. Object prehension (a); area of contact deformation and pressure distribution (b), (c).

Both compression and elongation strains are apparent and shown as internal pressure distributions in Fig. 8 (c). To simplify the analysis as much as possible, but to retain the essential features to be investigated, the vibration considered at a contact point is a finite-cubic block attached to a rigid wall by a simple spring and dashpot. The system is controlled by the frictional forces between the finite-cubic block and the moving belt upon which it is resting. This results in a simple one-degree-of-freedom structure with a non-linear excitation term. A similar analysis including a many-degrees-of-

freedom model for the wheel vibration, yet using only simple models for the friction, has been performed by Heckl and Abrahams [19]. The governing second order equation for this system is:

$$m\ddot{x} + r\dot{x} + sx = F(\dot{x}, \ddot{x}), \tag{3}$$

where *m* is the mass of the finite-cubic block, *s* is the spring constant, and *r* is the damping coefficient. The frictional force is given by $F(\dot{x}, \ddot{x})$, although it may be more natural to think of it as varying with time.

3.1. First Case: Grasp-Optimize-Replace

The governing equations for the contact surface, obtained by summing forces on the rider mass are:

$$\begin{aligned} m\ddot{x} + c_a(\dot{x} - \dot{x}_{ie}) + k_a(x - x_{ie}) &= F_G(t) \\ m\ddot{y} + c_s(\dot{y} - \dot{y}_{ie}) + k_s(y - y_{ie}) &= F_N(t) \\ F_G(t) &= \mu_D F_N(t) \ , \end{aligned} \tag{4}$$

where $F_N(t)$ is the fluctuating force normal to the tactile surface while $F_G(t)$ is the fluctuating frictional force. Anand [20] equates $F_N(t)$ to $F_G(t)$ using the reciprocal of μ_D as shown in (4). It is important to note that the deformation has a *y* component because some material passes underneath the contact which means that the sliding speed in *x* and the stain rate *y*, normal to the surface, are directly coupled [21].

$$m\ddot{y} + c_s(\dot{y} - \dot{y}_{ie}) + k_s(y - y_{ie}) = (m\ddot{x} + c_a(\dot{x} - \dot{x}_{ie}) + k_a(x - x_{ie}))/\mu_D \, .$$

When one of the contact points slips, the relationship between displacement and time will be approximated to a linear function [22].

In linear cases as mention by Howe [22], the slip displacement can be described as:

$$x = Ht \, , \tag{5}$$

where H is slope of Fig. 9. Substituting x from (5) into the right hand side of (4) gives:

$$m\ddot{y} + c_s(\dot{y} - \dot{y}_{ie}) + k_s(y - y_{ie}) = (c_a H + k_a Ht)/\mu_D \, . \tag{6}$$

The deformation surface between the object and tactile surfaces can be represented by $z^2 - 2py = 0$, and from Howell's definition [15] $\mu_D = KN^{\beta - 1}$, with $\beta = 2/3$ and $K = 1$. Then, the minimized form is:

$$m\ddot{y} + c_s(\dot{y} - \dot{y}_{ie}) + k_s(y - y_{ie}) = z^{2/3}(c_a H + k_a Ht) \text{ , and} \tag{7}$$

$$m\ddot{y} + c_s(\dot{y} - \dot{y}_{ie}) + k_s(y - y_{ie}) = A + Bt \, , \tag{8}$$

where $A = z^{2/3} c_a H$ and $B = z^{2/3} k_a H$.

The solution to the differential equation $\ddot{y} + \dot{y} + y = 0$ will be in the form: $y(t) = y_c(t) + y_p(t)$. Solving the integral equation gives the solution of $y_p(t)$ and $y_c(t)$ which becomes:

$y_p(t) = C_a Hz^{\frac{2}{3}}(t-1) + k_a Hz^{\frac{2}{3}}$ and $y_c(t) = C_1 e^{-\frac{t}{2}} \cos(\frac{\sqrt{3}}{2}t) + C_2 e^{-\frac{t}{2}} \sin(\frac{\sqrt{3}}{2}t)$ respectively.

In the case of a nonlinear or polynomial function, such as: $x = ae^{bt} + ce^{dt}$ or $x = at^n + bt^{n-1} + ... + p$ then the model nevertheless yields a single frequency solution. Pre-slip on some contact points (local slip) will appear before total slip occurs. This pre-slip can be detected by checking the oscillation frequency (fluctuation signal) and is identified as a pre-slip condition for the whole object. In the Grasp-Optimize-Replace experiment, the object was held between the robot gripper fingers. The robot would then decrease the prehension force until it could detect slip at some contact points which in turn would be indicative of complete slippage. The rule sets can be adapted by checking the oscillation frequency in the tactile array. If there exist some tactile elements having the same frequency of vibration, then whole pre-slip can be recognized.

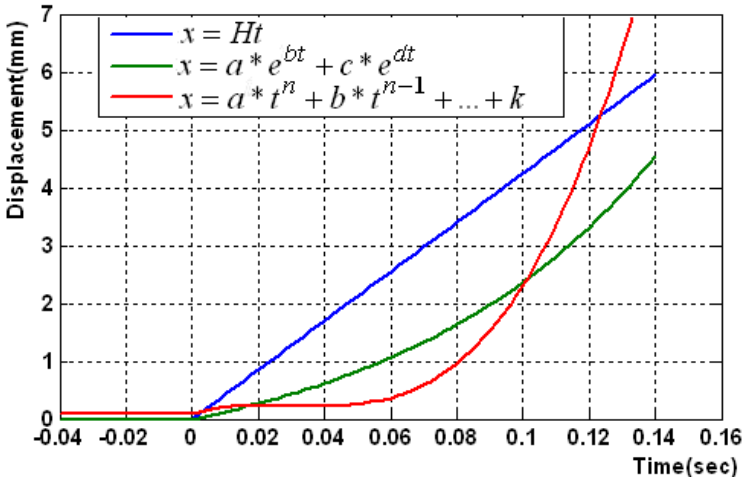

Fig. 9. Slip displacement functions.

3.2. Second Case: Grasp-Lift-Replace

In the second experiment, the deformation equation $z^2 - 2py = 0$ would not be correct any more because there exists an additional deformation of the contact surface when the robot tries to lift the object. Dundurs [23] presented the solution for the shear tractions, *S(x)* with dislocation distribution on an elastic material. He introduced geometry of the problem for elastic contacts as depicted in Fig. 10. The two components of force, shear force-*P(t)* and normal force-*Q(t)*, can vary independently and are introduced as shear traction. The contact between objects is separated into three zones corresponding to point locations along the x-axis. He described the shear traction based on the location of points in the slip zone (*a*) and stick zone (*b*) when they are dislocated.

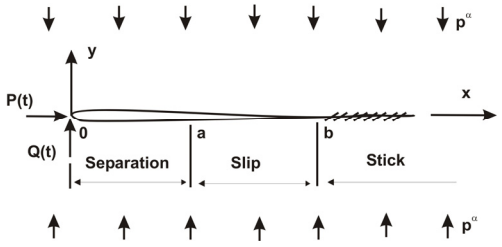

Fig. 10. Geometry of the problem by Dundurs [23].

Point locations *a* and *b* along the *x*-axis at initial distributions will be moved to locations a_1 and b_1 when variations in $P(t)$ and $Q(t)$ along the *x*-axis occur. Shear traction along the x-axis will simply be a function of x. By defining a set of regime (rules), Dundurs presented the existence of shear traction fluctuations as shown in Fig. 11.

From the conclusions made by Dundurs, this means there exists an extra term varying with time in the equations pertaining to surface deformation, i.e. $\sin(at)$. Then the equation of surface deformation, for example, will be $y = z^2/2p + \sin(at)$. With Howell's definition, the friction coefficient will be $\mu_D = K/\sqrt[3]{z^2/2p + \sin(at)}$ or $\mu_D = 1/\sqrt[3]{C + D\sin(at)}$, where $C = K^{-3}z^2/2p$ and $D = K^{-3}$. Equation (4) will become:

$$m\ddot{y} + c_s(\dot{y} - \dot{y}_{ie}) + k_s(y - y_{ie}) = \sqrt[3]{C + D\sin(at)}(c_a H + k_a Ht). \tag{9}$$

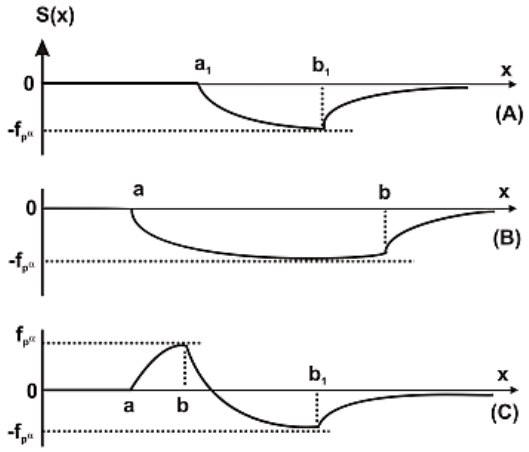

Fig. 11. Distributions of shear tractions for loading from (P1, Q1): (A)-Initial distribution; (B)-regime I; (C)-regime II (Regimes are defined by Dundurs [23]).

The same method can be used to find the solution to the differential equations, but $y_p(t)$ will be different.

$$y_p(t) = -y_1\int \frac{y_2 g(t)}{W(y_1, y_2)}dt + y_2\int \frac{y_1 g(t)}{W(y_1, y_2)}dt$$

where $g(t) = \sqrt[3]{C + D\sin(at)}(c_a H + k_a Ht)$,

$$y_1 = C_1 e^{-\frac{t}{2}}\cos(\frac{\sqrt{3}}{2}t),\ y_2 = C_2 e^{-t/2}\sin(\frac{\sqrt{3}}{2}t),$$

and $W(y_1, y_2) = \frac{\sqrt{3}}{2}C_1 C_2 e^{-\frac{t}{2}}$. Then, the solution will be

$$y_p(t) = -\frac{2}{\sqrt{3}}e^{-\frac{t}{2}}\cos(\frac{\sqrt{3}}{2}t)\int e^{\frac{t}{2}}\sin(\frac{\sqrt{3}}{2}t)\sqrt[3]{C + D\sin(at)}(A + Bt)dt + \frac{2}{\sqrt{3}}e^{-\frac{t}{2}}\sin(\frac{\sqrt{3}}{2}t)\int e^{\frac{t}{2}}\cos(\frac{\sqrt{3}}{2}t)\sqrt[3]{C + D\sin(at)}(A + Bt)dt \tag{10}$$

It may not be necessary to find the integral solution because the solution, $y_p(t)$, will always contain the term "$\sin(at)$". That means in slippage situations, there is always more than one oscillation frequency

(different numbers of fluctuation cycles) in the tactile array. One frequency is derived from the solution of $y_c(t)$, another from the solution of $y_p(t)$.

The alternating signals disperse throughout numerous tactile elements. When slip occurs, some of the elements give rise to signal changes. During prehension, the tactile sensor surface retracts in accordance to the object shape. Slip causing tangential force components affects only certain tactile elements. To rapidly measure the slip signal during prehension the computer memory may be organized in stacks. Locations T_1, T_2, ... T_n hold information from tactile sensors in the form of x-bar (average x-axis coordinate of force) and y-bar, vibrating cell, and vibration frequency. The subscript of T is the time of data collection - the number with the highest value in the stack being the most recent one. To compare stack data, indexes (pointers) called 'index 1' and 'index 2' are used to scan the data. Index 1 locates the starting point of the scan or the oldest stored data, whereas index 2 locates the finishing point of the scan or the current data. The data located by index 1 is compared with those located by index 2. Index 2 values are continually compared with Index 1 and decreased until the latest data is located. The location of index 1 is repeatedly scanned until index 2 locates the oldest stored data which means that the process is complete.

For the first experiment, there are three conditions which successfully indicate pre-slip. The first one is the differences in vibrating tactile element location determined by different stack pointers. The second one is the equal frequency of vibration determined by different stack pointers. The last condition is that the first two conditions are simultaneously true for both sides of the gripper. For the second experiment, there are four conditions, which indicate pre-slip if they are true. The first one is the inequality in the x-bar and y-bar coordinates determined by both stack pointers. The second one is the differences in vibrating tactile element location determined by different stack pointers. The third one is the frequency of vibration as determined by higher stack pointers being larger than that determined by lower stack pointers. The final condition is that the first three conditions are simultaneously true on any of the fingers.

4. Analysis of Results

The GOR experiment has been verified by the accelerometer chip to confirm the sensitivity of the proposed algorithm. As shown in Fig. 12, the accelerometer is attached on the surface of a grasped object. Whenever the grasped object slipped or moved from the gripper finger, the acceleration sensor would detect this. The output vibrations produced by an acceleration sensor and the display were then recorded while the robot decreased its grasping force. Overall, the response of the system was adequate for the purpose of testing the effectiveness of the proposed algorithm. The system is capable of logging the acceleration and it does this with a sample frequency of 200 Hz. The complete acceleration sensor is shown in Fig. 12 where the accelerometer is the small chip on the printed circuit board. The acceleration sensor, SCA3000 chip, is a three-axis accelerometer consisting of a 3D-MEMS sensing element. The sensor offers acceleration information via the SPI interface, and the measurement resolution is $0.75\,mm/s^2$. The measured response amplitude was flat within $\pm 2\ m/s^2$ across. There appeared to be severe mechanical vibrations or acceleration when the grasped object slipped from the finger gripper.

In observing ten trials of experimental results, it can be confirmed that the proposed algorithm is faster and more sensitive than the acceleration sensor. Warning of a potential slip situation was between three and six force decrements prior to release of the grasped object from the gripper. By use of a voice synthesizer, the robot vocally warns of pre-slip and then continues decrementing the prehension force until object release. Impressive is the fact that, despite its sensitivity, the acceleration sensor first detects movement at the point of total slip.

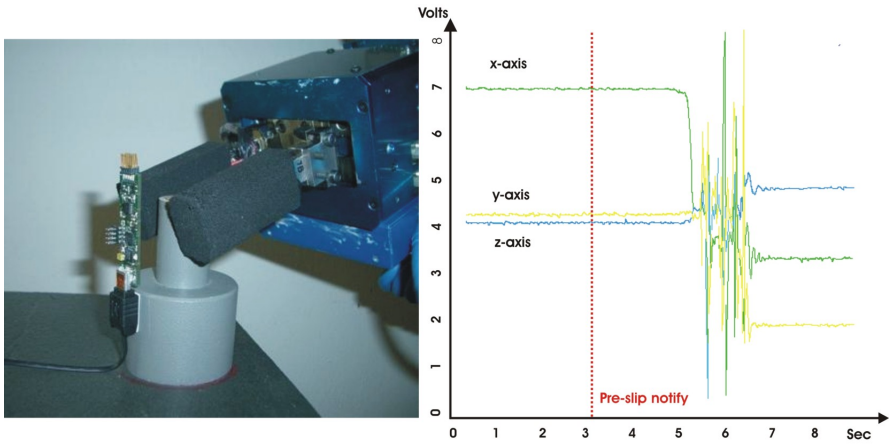

Fig. 12. The GOR experiment evaluated with the acceleration sensor.

In the GLR experiments, pre-slip detection applies while the prehended object is being lifted (Fig.13). The grasped object will slip relative to the gripper finger, but not to the earth, and hence two acceleration sensors are needed in this case. One accelerometer attached to the object is used to indicate the acceleration of the object relative to the earth. Another accelerometer is also attached to the tip of the robot finger, which indicates the acceleration of the robot finger relative to the earth. To detect slip between the object and the robot finger while lifting the object, the transformation between two different sensor coordinate frames is needed before the slip status can be found by comparison.

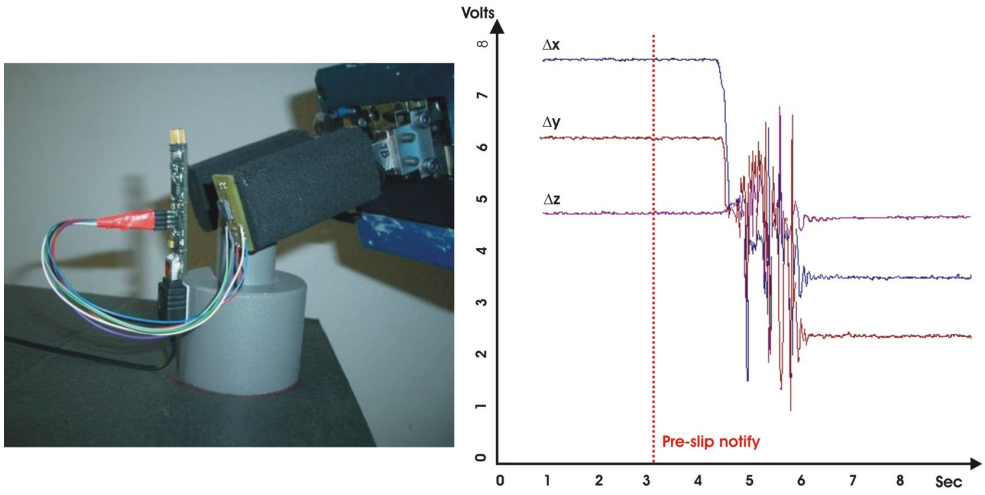

Fig. 13. The GLR experiments evaluated with the acceleration sensor.

The GLR experiment has been repeated ten times and yielded the same results as the GOR experiment. Every time the robot detects a pre-slip signal, it continues decreasing the grasping force until the object is released. Pre-slip detection always occurs between three and six decrements before total slip.

Point B of Fig. 14a is when the robot first senses pre-slip. Force is then increased until the tactile data increases to point C. If a pre-slip frequency is not sensed, the robot will prolong that degree of force while examining the response. At point D when the frequency at the tactile sensor surface meets the pre-slip conditions, the robot will increase the force until the sensed tactile data reaches point E. The lower graph of Fig. 14a exhibits the resulting frequency response sensed from all 64 tactile elements.

The final decision as to whether pre-slip has occurred or not depends on analysis of the complete data. Points B, C, and D in Fig. 14 a are found to have pre-slip, and the least possible force needed to lift the object shown by the tactile sensors is approximately 150 (dimensionless ADC data). The second experimental results are illustrated in Fig. 14b. At the outset, the robot will use a predetermined force to grasp the object. When the inner surface of the grippers make contact with the object and the tactile data are approximately 90 (dimensionless ADC data) at point A, the robot will decrease the prehension force, i.e. by incrementally increasing the distance between the fingers. The tactile data will gradually decrease to point B, upon which the frequency response will be sensed and follow the conditions described in the lower graph of Fig. 14 b. The lower graph of Fig. 14 b exhibits the results of the frequency response sensed from all 64 tactile elements.

To reach a decision as to whether a pre-slip condition has been reached or not requires another account as the sensed signals do not all result from pre-slip. For instance, they may result from the nature of the material used to develop the surface of the tactile sensors. Many tactile arrays are made from polymeric materials and many different types of foam are utilized. These have physical characteristic which differ enormously from those of rigid materials such as metals. Slow shape restoration results in unstable foam mass, causing the frequency response to fluctuate. Hence, the response does not result from pre-slip, but from the characteristics of the tactile sensor surface material. From the behavior of the localized contacts between tactile sensor and object surfaces, the minimum force cannot be determined by a unidirectional increase or decrease in applied force.

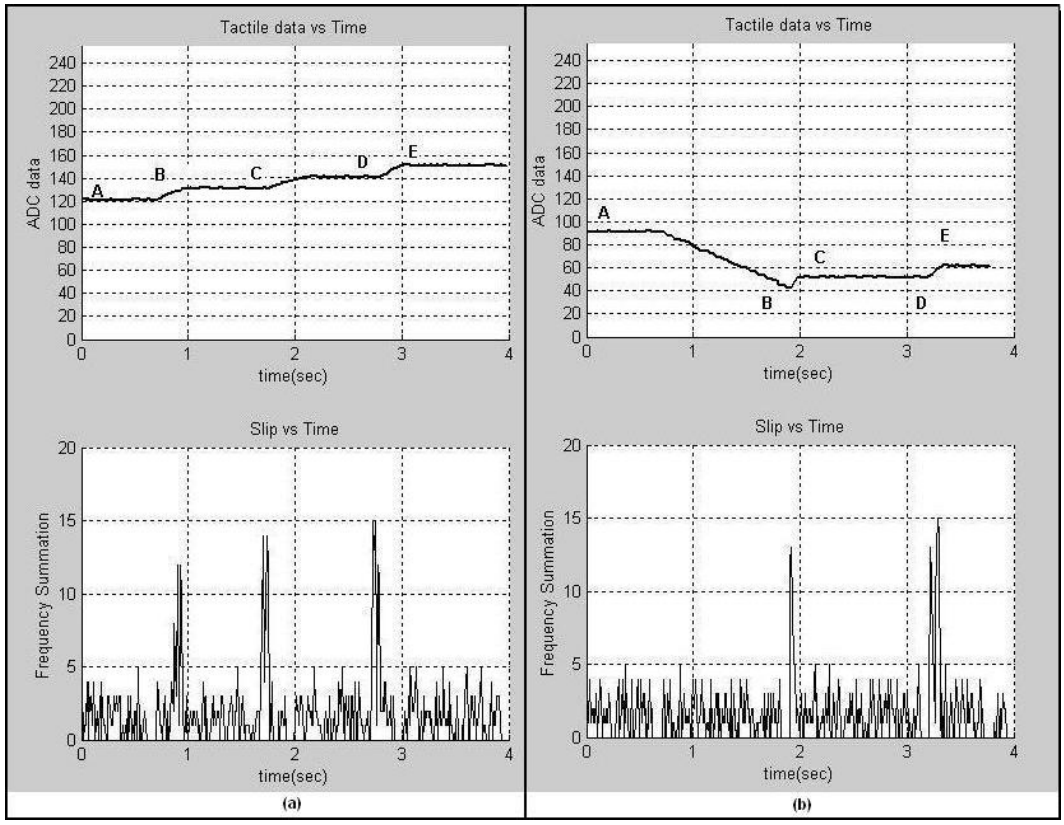

Fig. 14. Minimum prehension force determined by increasing and decreasing applied force.

This means the same degree of force exerted at different times will result in different prehension stabilities. To exemplify, at a certain point in time the force at point E lies between that at point A and C and is adequate for object prehension without pre-slip. The force required to retain the object now must be equal to or greater than that at point E.

5. Conclusions

Tactile sensing elements can acquire force feedback information at the contact points between a grasped objects and the tactile surface. The tactile sensor is capable of measuring near static acceleration which is interesting to investigate. A proposed method for calibrating the tactile data to predict slip is extremely useful. The advantage of this method is that the acquisition of direct contact forces provides grasping force adaptability in addition to optimum prehension by determining the necessary minimum applied force. With respect to real applications, the manipulation of fragile components or assemblies requires precise force control under conditions of varying acceleration. The force feedback information from the tactile surfaces used in this work can be used to optimize gripper alignment and achieve object prehension and manipulation with using minimum retention force. This procedure can be restructured in such a way that the orientation of an object, with respect to a gripper, can be determined regardless of its identity. Minimum prehention forces are ascertained with respect to its desired stable orientation. However, where objects of differing size and geometry are used, a different scanning speed may be necessary. For examples, heavier objects need the shorter processing loop times in order to adjust the minimum force. Comprehensive details about the prototype sensor, data acquisition and processing principles together with incorporated mathematical derivations for part pre-slip sensing are provided in a previously published work [24].

References

[1]. D. P. J. Cotton, A. Cranny, N. M. White, P. H. Chappell and S. P. Beeby, A Novel Thick-Film Piezoelectric Slip Sensor for a Prosthetic Hand, *IEEE Sensors Journal*, 7, 5, 2007, pp. 752-761.

[2]. D. S. Childress, Historical aspects of powered limb prosthesis, *Clinical Prosthetics and Orthotics,* 9, 1985, pp. 2-13.

[3]. Y. Yamada, Hiroyuki Morita, and Yoji Umetani, Slip phase isolating: impulsive signal generating vibrotactile sensor and its application to real-time object regrip control, *Robotica,* 18, 1, 2000, pp. 43-49.

[4]. C. Melchiorri, Slip detection and control using tactile and force sensors, *Mechatronics,* IEEE/ASME Transactions, 5, 3, 2000, pp. 235–243.

[5]. Schunk GmbH & Co, catalogue "SCHUNK_Automation_Modulare_Robotik_DE_EN. pdf", available at: http://www.schunk.com/schunk/index.html

[6]. R. S. Johansson and G. Westling, Roles of glabrous skin receptors and sensorimotor memory in automatic control of precision grip when lifting rougher and more slippery objects, *Exp. Brain Res.,* 56, 1984, pp. 550-564.

[7]. G. Westling and R. S. Johansson, Factors influencing the force control during precision grip, *Exp. Brain Res.,* 53, 1984, pp. 277-284.

[8]. G. Cadoret and A. M. Smith, Friction, not texture, dictates grip forces used during object manipulation, *Journal Neurophysiol,* 75, 1996, pp. 1963-1969.

[9]. R. D. Howe and M. R. Cutkosky, Sensing Skin Acceleration of Slip and Texture Perception. *IEEE International Conference on Robotics and Automation*, 1989, p. 145-150.

[10]. R. D. Howe and M. R. Cutkosky, Practical force-motion models for sliding manipulation, *International Journal of Robotics Research,* 15, 6, 1996, pp. 557–572.

[11]. R. D. Howe and M . R. Cutkosky, Dynamic Tactile Sensing: Perception of Fine Surface Features with Stress Rate Sensing, *IEEE Trans on Robotics and Automation,* 9, 2, 1993, pp. 140-151.

[12]. G. E. Dieter, Metalurgia Mecânica, *Mc Graw Hill Inc*. 1981.

[13]. D. Dowson, History of Tribology, *Longman Inc*., New York, 1979.

[14]. B. Lincoln Br. J., Frictional and elastic properties of high polymeric materials, *Apply Physics,* 3, 1952, pp. 260-263.

[15]. H. G. Howell and J. Mazur, Amontons' Law and Fibre Friction, *Journal of the Textile Institute,* 1953, pp. 59-69.

[16]. A. Krawietz, Materialtheorie, Mathematische Beschreibung des phdnomenologischen thermomechanischen Verhaltens, *Springer-Verlag*, Berlin, 1986.

[17].R. A. Ibrahim, Friction-induced vibration, chatter, squeal, and chaos: Part i-mechanics of contact and friction, *Applied Mechanics Reviews,* 47, 1994, pp. 209-226.
[18].D. Godfrey, Vibration reduced metal-to-metal contact and causes an apparent reduction in friction, *ASLE Transactions,* 10, 1967, pp. 183-192.
[19].M. A. Heckl and I. D. Abrahams, Active control of friction-driven oscillations, *Journal of Sound and Vibration,* 193, 1996, pp. 417-426.
[20].A. Anand and A. Soom, Roughness-Induced Transient Loading at Sliding Contact During Start-Up, *Journal of Tribology,* 106, 1984, pp. 49-53.
[21].W. P. Vellinga and C. P. Hendrinks, Sliding friction dynamics of hard single asperities on soft substrates, *Physic Review,* 63, 2001, pp. 12-14.
[22].R. D. Howe and M. R. Cutkosky, Sensing Skin Acceleration of Slip and Texture Perception, *IEEE International Conference on Robotics and Automation*, 1989, pp. 145-150.
[23].J. Dundurs and M. Comninou, An Education Elasticity Problem With Friction, Part3: General Load Paths, *Journal of Applied Mechanics,* 50, 1983, pp. 77-84.
[24].S. Petchartee, G. Monkman, Slip Prediction through Tactile Sensing. In: *Proc. 2007 International Conference on Sensing Technology*, New Zealand, 2007.

Guide for Contributors

Aims and Scope

Sensors & Transducers Journal (ISSN 1726-5479) provides an advanced forum for the science and technology of physical, chemical sensors and biosensors. It publishes state-of-the-art reviews, regular research and application specific papers, short notes, letters to Editor and sensors related books reviews as well as academic, practical and commercial information of interest to its readership. Because it is an open access, peer review international journal, papers rapidly published in *Sensors & Transducers Journal* will receive a very high publicity. The journal is published monthly as twelve issues per annual by International Frequency Association (IFSA). In additional, some special sponsored and conference issues published annually.

Topics Covered

Contributions are invited on all aspects of research, development and application of the science and technology of sensors, transducers and sensor instrumentations. Topics include, but are not restricted to:

- Physical, chemical and biosensors;
- Digital, frequency, period, duty-cycle, time interval, PWM, pulse number output sensors and transducers;
- Theory, principles, effects, design, standardization and modeling;
- Smart sensors and systems;
- Sensor instrumentation;
- Virtual instruments;
- Sensors interfaces, buses and networks;
- Signal processing;
- Frequency (period, duty-cycle)-to-digital converters, ADC;
- Technologies and materials;
- Nanosensors;
- Microsystems;
- Applications.

Submission of papers

Articles should be written in English. Authors are invited to submit by e-mail editor@sensorsportal.com 6-14 pages article (including abstract, illustrations (color or grayscale), photos and references) in both: MS Word (doc) and Acrobat (pdf) formats. Detailed preparation instructions, paper example and template of manuscript are available from the journal's webpage: http://www.sensorsportal.com/HTML/DIGEST/Submition.htm Authors must follow the instructions strictly when submitting their manuscripts.

Advertising Information

Advertising orders and enquires may be sent to sales@sensorsportal.com Please download also our media kit: http://www.sensorsportal.com/DOWNLOADS/Media_Kit_2008.pdf